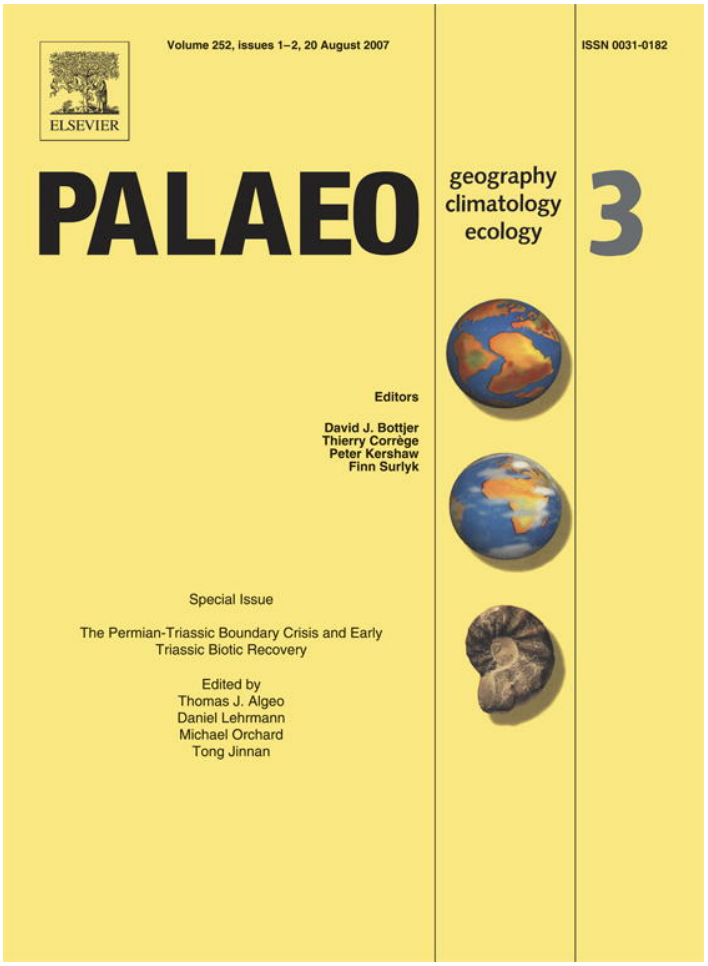

Available online at www.sciencedirect.com
ScienceDirect
PALAEO
Palaeogeography, Palaeoclimatology, Palaeoecology 252 (2007) 239–258
www.elsevier.com/locate/palaeo

Sedimentary evidence of Early–Late Permian mid-latitude continental climate variability, southern Bogda Mountains, NW China

Wan Yang [a,*], Yiqun Liu [b], Qiao Feng [c], Jinyan Lin [b], Dingwu Zhou [b], Dan Wang [b]

[a] *Department of Geology, Wichita State University, Wichita, KS 67260, USA*
[b] *Department of Geology, Northwestern University, Xian, China*
[c] *College of Geoinformation Science and Engineering, Shangdong University of Science and Technology, Qingdao, China*

Accepted 30 November 2006

Abstract

A preliminary Early–Late Permian mid-latitude continental climatic record in NW China was interpreted mainly from sedimentary climate indicators and type and stacking pattern of depositional systems and cycles in a 1178-m fluvial–lacustrine section. Depositional systems analysis delineated five types of primary fluvial and lacustrine depositional cycles, which were grouped into three (high, intermediate, and low) orders. Semi-arid, subhumid, and humid climate types in terms of relative precipitation/evaporation ratio were interpreted and climate variability was identified at sub-cycle and high, intermediate, and low-order cycle scales. Early Kungurian climate fluctuated between subhumid to humid and middle–late Kungurian climate shifted gradually from subhumid/semi-arid to semi-arid. Roadian climate fluctuated widely from humid to semi-arid with strong precipitation seasonality at sub-cycle and high-order cycle scales. Wordian climate was dominantly humid with short subhumid intervals and ended with a peak semi-arid condition. Capitanian climate was mainly subhumid to humid, as the start of a long interval of dominantly humid, strongly wet–dry conditions into the Wuchiapingian time. The late Kungurian–Wordian semi-arid condition is incompatible with modern mid-latitude east-coast humid climate, suggesting different mechanisms operating in Pangea and Panthalassa. The highly variable Roadian–Wordian climate may have started terrestrial mass extinction that climaxed at the end of Permian.

Keywords: Early to Late Permian; Continental climate; Fluvial; Lacustrine; China

1. Introduction

The pace and cause(s) of end-Permian mass extinction are still in debate (e.g., Erwin, 1993; Knoll et al., 1996; Isozaki, 1997; Erwin, 2002; Ward et al., 2005). A global cause would have had a significant impact on continental ecological and climatic conditions. Thus, the Permian continental climate history is critical to understanding the causes and processes of end-Permian mass extinction. We report a preliminary Early–Late Permian mid-latitude continental climate record in NW China, interpreted from mainly

* Corresponding author.
E-mail address: wan.yang@wichita.edu (W. Yang).

0031-0182/$ - see front matter © 2007 Elsevier B.V. All rights reserved.
doi:10.1016/j.palaeo.2006.11.045

sedimentary climate indicators, including lithology, paleosols, depositional systems, and depositional cyclicity. Four levels of climate variability at 0.1–100-m scales were identified. The record is a start of detailed reconstruction of Permo–Triassic continental climate in NW China. Our work also shows the feasibility of

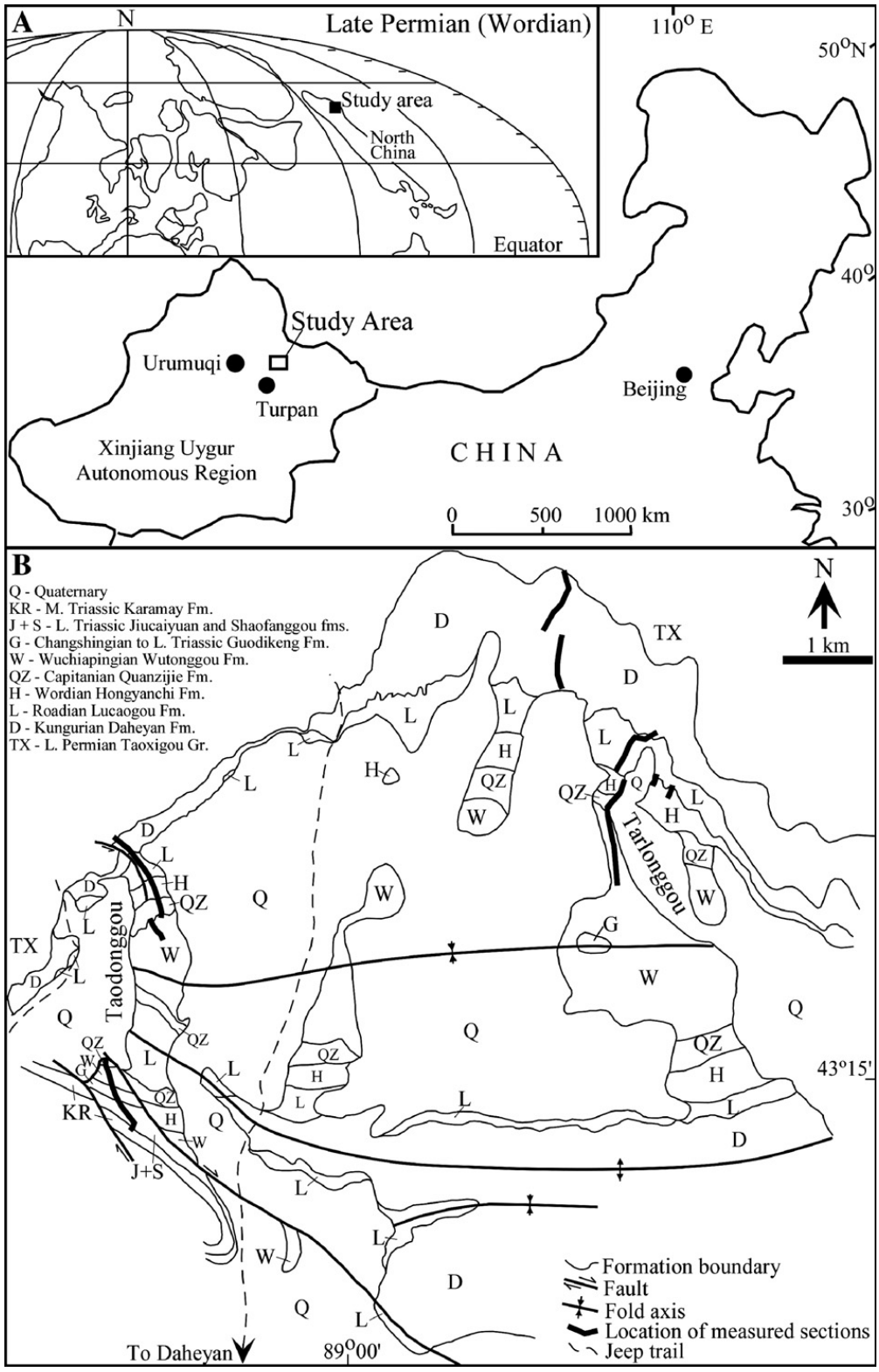

Fig. 1. (A) The study area in Xinjiang, NW China, was located at ~50°N in Wordian (Kazanian) time (inset; Scotese and McKerrow, 1990, modified from Brand et al., 1993) and migrated northward from ~40 to 50°N during Kungurian to Wuchiapingian (Ziegler et al., 1997). (B) Geological map showing Tarlong and Taodonggou sections in a syncline in southern Bogda Mountains.

reconstructing continental paleoclimate using mainly sedimentary evidence.

1.1. Geological background

The study area is located in Tarlonggou, southern Bogda Mountains, NW China (Fig. 1). A 1178-m Lower–Upper Permian superbly-exposed section was measured at a cm–dm scale and a 50-km^2 area was mapped. Thin-section petrography of 104 sandstone, limestone, mudrock, and paleosol and analysis of total organic carbon content and kerogen type of 79 mudrock and carbonate samples were conducted.

The Permian rocks were deposited in intermontane rift basins on the Carboniferous–basal Permian volcanic-arc basement formed by collision between Junggar and Northern Tian Shan plates (Allen et al., 1995). Kungurian fluvial deposits overlie unconformably volcanoclastics of Artinskian Taoxigou Group (Figs. 2, 3A; Liao et al., 1987; Wartes et al., 2002). Upper Permian–Lower Triassic thick fluvial and lacustrine rocks were probably deposited in the late rifting to thermally driven drift phase (cf. Carroll et al., 1995; Shao et al., 1999). Lake expansion and contraction and provenance uplift to the south (e.g., Shao et al., 2001; Wartes et al., 2002; Greene et al., 2005) had occurred episodically in the region during Permian. Permo–Triassic chronostratigraphy in the study area was correlated by geological mapping and physical tracing of the measured strata to nearby Taodonggou section, where litho- and bio-stratigraphy was well established (e.g., Zhang, 1981; Liao et al., 1987; Wartes et al., 2002; Zhu et al., 2005; Yang et al., 2006; Figs. 1, 2).

1.2. Steps of climate interpretation

A wealth of climate information was recorded by lithofacies and their stacking patterns. Paleoclimate interpretation took three steps in this study (Fig. 4). First, depositional environments and systems of lithofacies were interpreted using field and laboratory data. Systematic and repetitive changes of depositional environments define three orders (high, intermediate, and low) of depositional cycles. Second, major processes controlling cyclic sedimentation, such as tectonic, climatic, and autogenic processes intrinsic to specific environments were interpreted. Tectonic influence on intermontane sedimentation is significant (e.g., Wartes et al., 2002). Thus, movement of provenance and lake spilling point, subsidence at the depositional site, and their possible effects on lithofacies and depositional environment changes were interpreted and filtered prior to climate interpretation (Fig. 4). Last, climate was interpreted as arid, semi-arid, subhumid, and humid in terms of precipitation (P)/evaporation (E) ratio, using sedimentary evidence within high-order cycles. Subsequently systematic changes of P/E ratio over successive high-order cycles define intermediate and low-order climate variability.

2. Lithofacies and depositional systems

2.1. Conglomerate

Most conglomerates in the study area are clast-supported with very coarse–coarse sand matrix. Clasts are dominantly andesitic and basaltic, increasingly

System	Series		Stage	Lithostratigraphy	Cyclostratigraphy (this study[a])		
					Low-order cycles	Thickness (m)	No. of IC/HC[b]
Permian	Upper	Lopingian	Changshingian	Guodikeng Fm.			
			Wuchiapingian	Wutonggou Fm.	Wutonggou LC (top not reached)	428.6	9/123
	Middle	Guadalupian	Capitanian	Quanzijie Fm.	Quanzijie LC	67.5	2/8
			Wordian	Hongyanchi Fm.	Hongyanchi LC	116.7	8/45
			Roadian	Lucaogou Fm.	Lucaogou LC	179.6	11/136
	Lower	Cisuralian	Kungurian	Daheyan Fm.	U. Daheyan LC	91.1	1/12[c]
					M. Daheyan LC	188.5	1/16[c]
					L. Daheyan LC	106.5	6/32
			Artinskian	Taoxigou Gr.			

a. Wavy boundaries are significant unconformities identified in this study.
b. Number of intermediate-order/high-order depositional cycles.
c. Minimal counts of high-order cycles because high-order cycles in some thick braided stream deposits were not differentiated (Fig. 5).

Fig. 2. Synthesized chrono- and bio-stratigraphy (Zhu et al., 2005) and cyclostratigraphy. The Wutonggou low-order cycle is incomplete; field reconnaissance and correlation with the Taodonggou section indicate that ~300 m of strata remain to be measured, which have similar depositional systems to the measured part. The low-order depositional cycles are named after relatively correlative lithostratigraphic formations.

sedimentary in Upper Permian, and are mainly granule–pebble-sized, decreasing in maximum size and amount in Upper Permian. They are subangular to rounded, moderately sorted, and commonly imbricated. Planar, cross, and graded beddings are common. This facies is commonly lenticular with internal and basal erosional

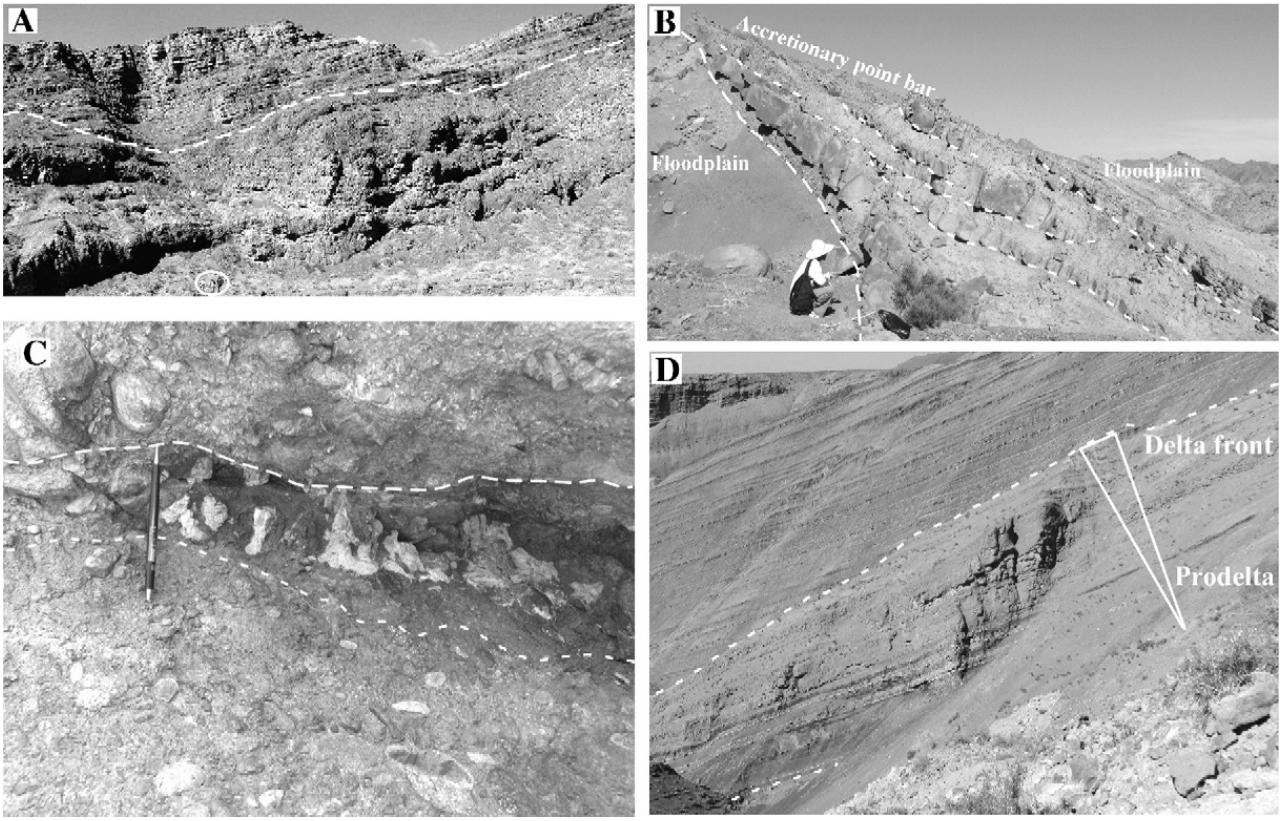

Fig. 3. (A) An unconformity separating volcanoclastic debris flow deposits of the Taoxigou Group from the overlying braided stream high-order cycles (HCs) of the Lower Daheyan low-order cycle (LC). People (circled) are 1.7 m tall. (B) An upward-fining classic meandering stream HC composed of accretionary point bars (outlined by short-dashed lines) with an erosional base (long-dashed line) in the lower Wutonggou LC. Person is 1 m tall. (C) A Calcisol in the Upper Daheyan LC underlies crudely tabular cross-bedded braided stream conglomerate with an erosional contact (long-dashed line) and contains elongate subvertical calcitic nodules overlying conglomerate containing reddened illuvial sands with a digitated and diffuse boundary (short-dashed line). Pencil is 15 cm long. (D) A lacustrine deltaic HC in the Lucaogou LC. Triangle shows the upward-coarsening and thickening trend. The HC is 6 m thick and encased in a thick succession of lacustrine mixed carbonate and siliciclastic HCs in the background. (E) Two lacustrine mixed carbonate and siliciclastic HCs in the Lucaogou LC composed of transgressive littoral to sublittoral fine sandstone, siltstone, and silty shale (a), maximum-expansion profundal organic-rich shale (b), regressive limestone (c) and laminated dolomite and dolomitic shale (d). Dashed lines are HC boundaries. Pencil (circled) is 15 cm long. (F) Microphotograph of dolomitic shale in a lacustrine mixed carbonate and siliciclastic HC in the Lucaogou LC, showing sub-mm laminae of dolomite (a), organic-rich mixed clay and calcite (b), organic-poor limestone (c), organics (d), and dolomite crust (not shown in the photo). Calcite is stained red. Brown micritic dolomite laminae are common, with sharp top and base. Internal wavy discontinuous organic partings suggest algal influence during dolomite precipitation. Organic laminae are common, thin, and discontinuous. Organic-rich mixed clay and calcite laminae are common and have sharp base and diffuse top and sparse burrows. Organic-poor limestone laminae are uncommon and poorly defined. Dolomitic crust is not uncommon and persistent in thickness, has sharp top and base, and contains common vertical microscopic tubules and sparse quartz grains, suggesting syndepositional dolomite precipitation. Fine-sand and silt quartz grains (clear-colored) scatter throughout and are angular to subrounded, probably of an eolian origin. Clasts of sandstone (white arrow) and elongate, angular, bedding-parallel limestone (black arrow) and dolomite crust are common and are likely rip-up clasts. A limestone clast in the lower part contains domal chambers with dolomitized walls and micritic calcite infill of a probable microbial/stromatolitic origin. The chamber size increases downward, suggesting that the clast is overturned. The clast ruptures underlying dolomitic laminae and is covered conformably by limestone and organic laminae, suggesting that the clast is a dropstone probably from melting lake ice. Dropstones of this and other types are present throughout the sample. Interlamination of different types of laminae suggests high-frequency lake-level oscillation. Two through-going white lines are artificial fractures. Sample TR50–6, plane light. (G) Two stacked Calcisols with well-defined Bk and Bt horizons (outlined by short-dashed lines) overlie conformably (long-dashed line) a skeletal wackestone in the uppermost Hongyanchi LC. Person is 1.75 m tall. (H) Abundant iron-oxide pisoids (arrows) in mm-cm-size equant peds of the Bs horizon of a Spodosol in the Wutonggou LC. Pencil is 15 cm long. (I) An unconformity (long-dashed line) separating the mixed carbonate and siliciclastic lacustrine HCs in the Lucaogou LC (left) from braided stream and coarse-grained meandering stream HCs of the Hongyanchi LC (right, outlined by short-dashed lines). People (circles) are 1 m tall.

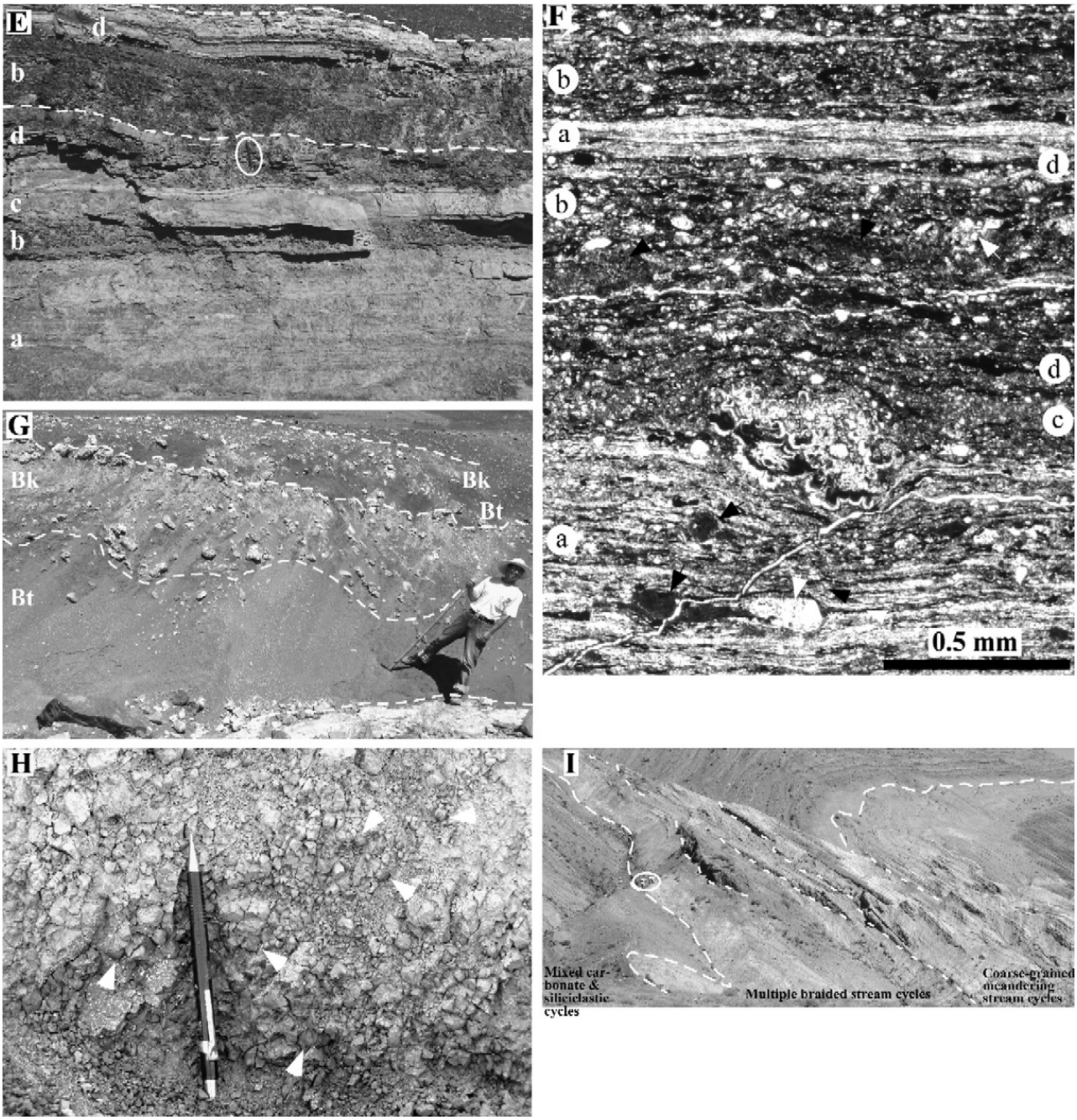

Fig. 3 (*continued*).

surfaces and interbedded with conglomeratic sandstones. Some conglomerates are persistent, 10 cm thick and 10 m–300 m long, and well sorted with sharp and even base and top.

Conglomerates in the lower part of upward-fining intervals were interpreted as channel bar deposits of braided streams where they have a shallow (1–10 cm) erosional base and are not overlain by muddy overbank deposits, and as channel lag and lower point bar deposits of meandering streams where they have a high-relief (10–100 cm) erosional base and are overlain by muddy overbank deposits (Fig. 4). Laterally persistent thin conglomerates were interpreted as high-energy, well-washed lakeshore deposits (i.e. shoreline pebbles) on the basis of their association with underlying paleosols and overlying well stratified and well sorted littoral arenites (Fig. 4).

Matrix-supported conglomerate is rare. Clasts are dominantly igneous, granule to boulder-sized, very poorly sorted, very angular, and lack of preferred orientation and vertical grain size trend. They are 1–7 m thick, 10 m–100 m long, with a sharp non-

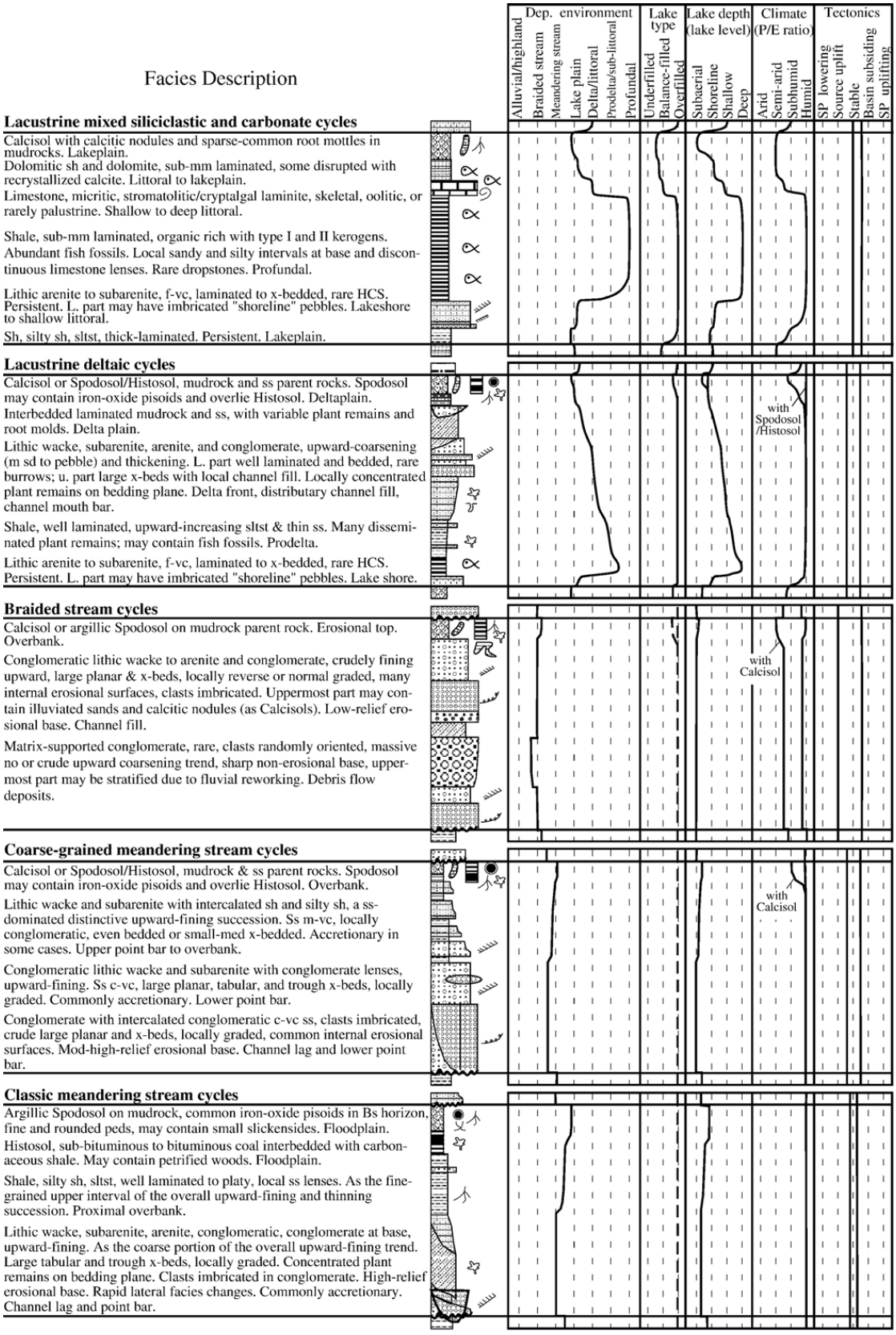

Fig. 4. Lithology, sedimentary structures, and interpretations of five basic types of primary HCs. Each type has several varieties because commonly not all the facies are present in a particular cycle. No vertical scale intended. Interpretation begins with depositional environment, lake depth, lake type (speculative for non-lacustrine cycles), tectonics, and ends with climate. Climate interpretation also considers the type and stacking pattern of vertically adjacent HCs. See Figure 5 for explanation of lithologic symbols.

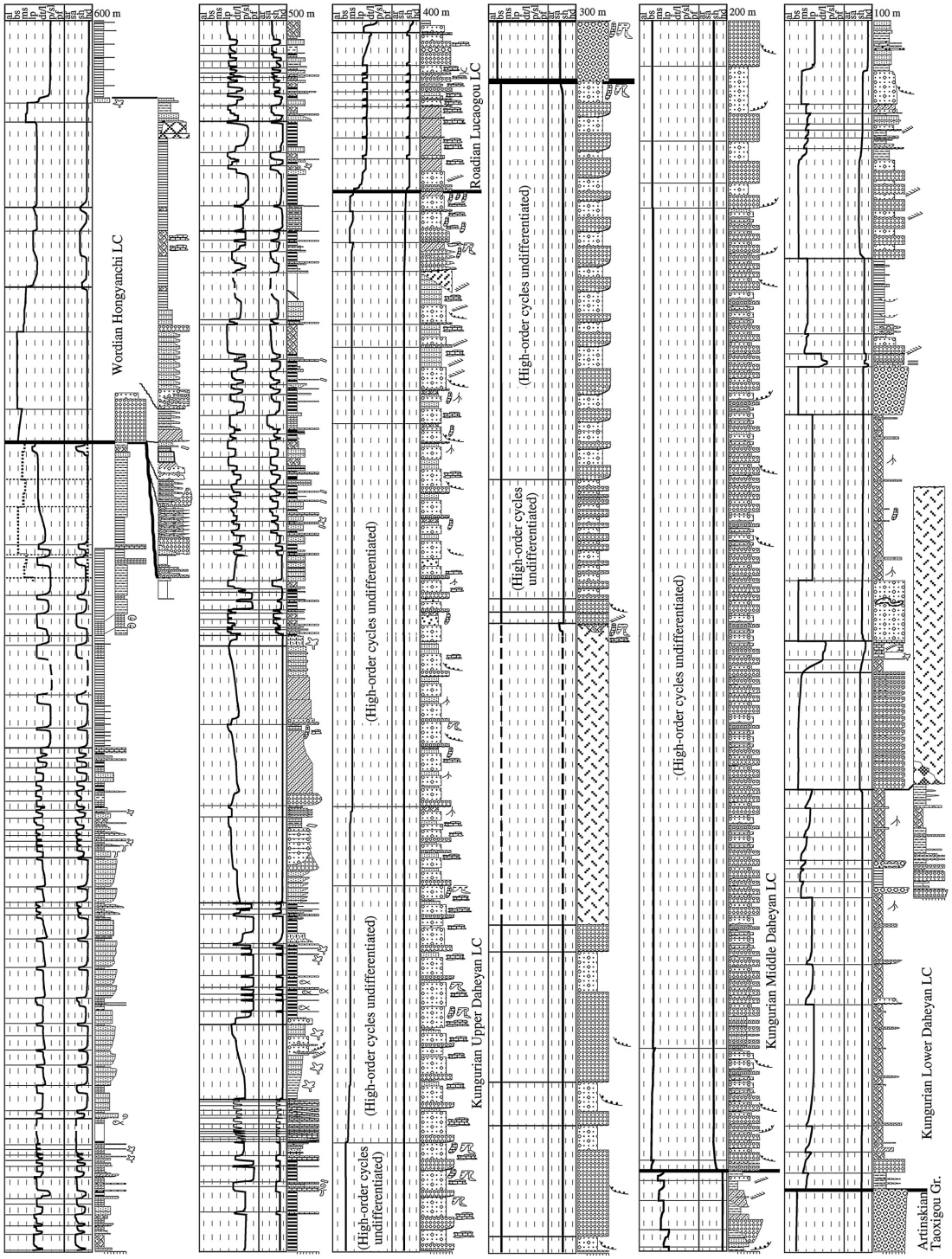

Fig. 5. Lithology, sedimentary structures, and interpretations of depositional environments and cycles, and climate variability of Lower–Upper Permian Tarlong section. Dashed curves are for igneous or covered intervals; dotted curves and cycle boundaries for erosional overlap.

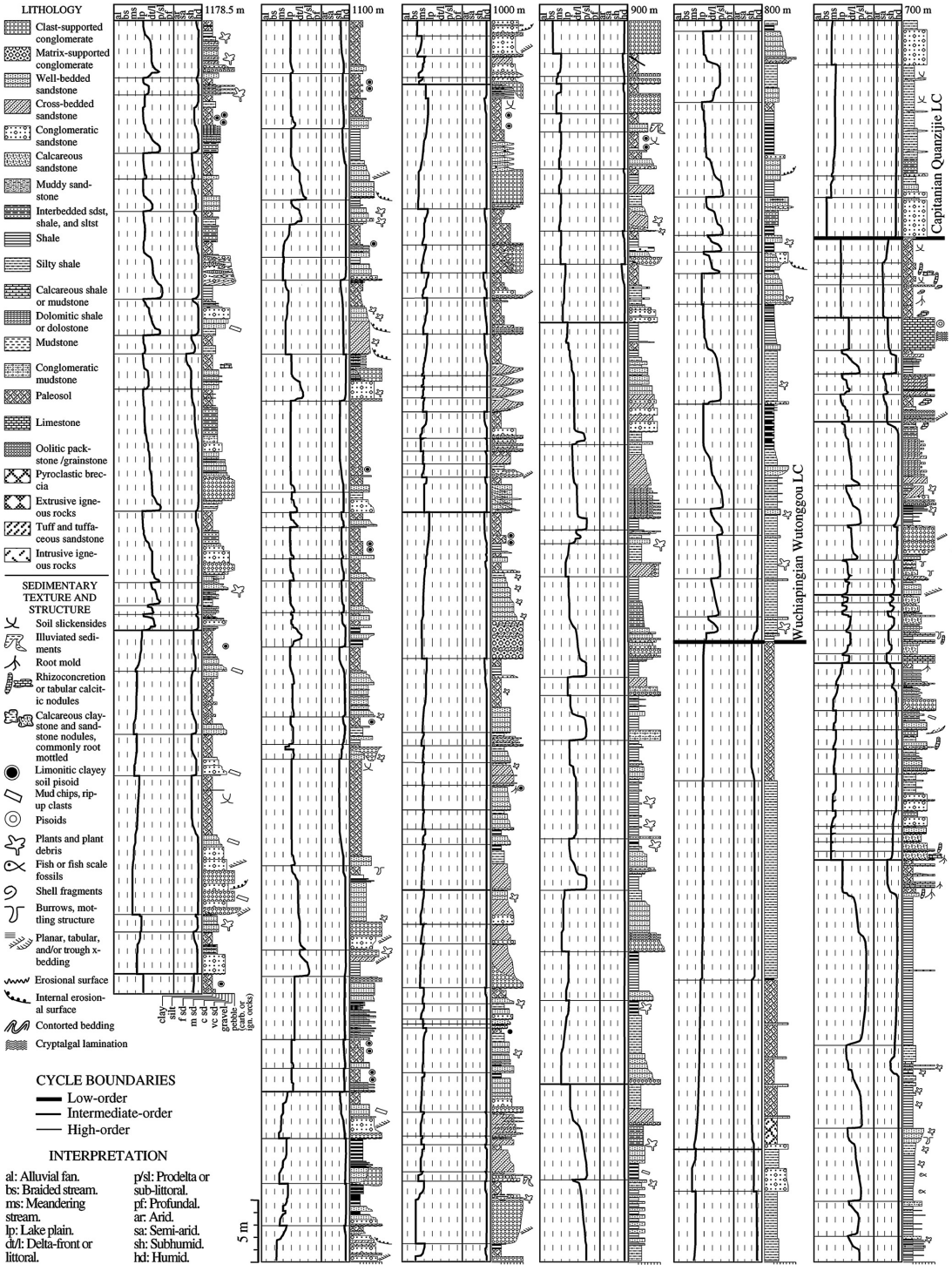

Fig. 5 (*continued*).

erosional base and no internal erosional surfaces, and occur mainly as isolated units within thick braided stream deposits. They were interpreted as debris flow deposits (Fig. 4).

2.2. Sandstone

Lithic wacke and subarenite are the most common in the study area. Lithic grains are dominantly igneous and increasingly sedimentary upward. Feldspars are commonly $<25\%$ and quartz 0–5%. Grains are mainly coarse–very coarse, subangular to subrounded, and poorly to moderately sorted. Gravels are common in Lower Permian, decreasing to $<10\%$ in Upper Permian. Planar, cross, and graded beddings are common; hummocky cross stratification is rare. Some sandstones are massive and mottled and, in some cases, change upward and laterally gradationally into sandy mudrocks.

Sandstones in the lower part of upward-fining intervals are commonly lithic subarenite to wacke with large-scale beddings, lenticular or accretionary, and commonly overlie conglomerate. They were interpreted as point bar deposits (Figs. 3B, 4). Those in the upper part are thin (10 cm), laterally persistent, interbedded with mudrocks, and were interpreted as overbank deposits. Massive sandstones in the upper part of fluvial (mainly braided stream) deposits commonly contain nodular or tabular micrite and were interpreted as paleosols (Fig. 3C). Well-bedded, laterally persistent lithic subarenite and arenite may be hummocky cross stratified, contain scattered superficial ooids, and are associated with limestones and well-laminated shale; they were interpreted as high-energy littoral lacustrine deposits (Fig. 4). Some thin (1–10 cm), laterally persistent wackes have disrupted bedding with relict laminations and abundant grayish green mm-size root molds; they overlie littoral sandstone, shale, or carbonate, and were interpreted as sheet flow deposits on lakeplain. Finally, laterally persistent lithic wacke to arenite in upward-coarsening and thickening intervals were interpreted as delta-front deposits (Figs. 3D, 4).

2.3. Mudrock

Mudrocks include siltstone, shale, and massive mudstone. Thick-laminated siltstone and shale are commonly interbedded with thin sandstones; some are plant-rich or carbonaceous; others are disrupted by vertical to subvertical mottles. Sub-mm-laminated shales in the Lucaogou low-order cycle (LC) are dolomitic or organic-rich (Figs. 2, 3E, 3F, 4, 5). Dolomitic shales have alternating dolomitic and clayey or silty organic-rich laminae. Euhedral to anhedral dolomite rhombs are 10 μm large. Organic-rich shales have alternating silty and clayey laminae with types I and II kerogens. Both shales contain locally concentrated well-preserved fossil fish with ostracods and chonchostracods. Massive mudstones occur throughout the section (see Paleosols).

Siltstone and shale in upper part of upward-fining and thinning intervals were interpreted as overbank or deltaplain deposits (Figs. 3B, 4). Some carbonaceous shales overlain by persistent shoreline and littoral sandstone or conglomerate were interpreted as lakeplain swamp deposits. Those with disseminated plant remains and intercalated sandstones in the lower part of upward-thickening and coarsening intervals were interpreted as prodeltaic deposits (Figs. 3D, 4).

The association of sub-mm laminated shale with limestone suggests a low-energy lake environment lack of coarse siliciclastic supply. Discontinuous, isolated gravel and sand in some shale distort or rupture underlying laminae and are overlain by continuous laminae (Fig. 3F). They were interpreted as dropstones deposited when seasonal lake ice melted. Mud and organic-rich laminae in dolomitic shale suggest increased mud influx, probably during wet seasons, whereas dolomitic laminae suggest reduced mud influx and increased evaporation (e.g., Carroll, 1998), probably during dry seasons (Fig. 3F). Interlaminated clay-rich and silt-rich laminae in organic-rich shale may have a similar origin, where clay-rich laminae were deposited during dry or icy seasons and silt-rich laminae in wet seasons. Dolomitic shale commonly overlies organic-rich shale, suggesting that the latter was deposited in a deeper profundal lake than the former (Figs. 3E, 4).

2.4. Limestone

Oolitic and skeletal grainstone to wackestone and micrite are far less abundant than siliciclastic rocks. Oolites contain ooids with radial and/or concentric cortices and mostly lithic cores, and a variable amount of sand–pebble-sized lithic grains. They are evenly bedded, 5–40 cm thick, and laterally persistent. Skeletal limestones are commonly arenaceous, well bedded, and persistent. Those in basal Lucaogou LC form a 5-m thick interval of northward-prograding clinoforms (Fig. 5). Those in upper Hongyanchi LC are interbedded with arenite and subarenite and contain well-preserved bivalves (Fig. 5). Algal and stromatolitic laminites in the Lucaogou and Hongyanchi LCs are 5–30 cm thick. Sub-mm organic-rich laminae alternate with partially dolomitized micritic

laminae. Laterally linked stromatolitic beds are commonly associated with dolomitic shale and recrystallized micrite. Last, thin (5–20 cm), well bedded to lenticular micrite occurs in high-order cycles (HCs) of the Lucaogou LC. They contain sub-mm organic-rich shale laminae and locally abundant fossil fish, and are highly recrystallized with micro-brecciation and cone-in-cone structures. Some are highly mottled to form a nodular texture.

Skeletal limestones were probably deposited in shallow well-oxygenated lakes; oolites in high-energy littoral environment; stromatolitic laminites in very shallow quiet environment; and finely laminated organic-rich micrites in sub-littoral environment. The highly altered and mottled micrite is probably palustrine or pedogenically altered lacustrine deposits.

2.5. Paleosols

Three types of paleosols were identified. Calcisols (Mack et al., 1993) contain equant, elongate, to tabular, autobrecciated micritic nodules, with scattered lithic grains and patchy mud. Discontinuous concentric micritic laminae may be present. Sparry calcite-filled rounded molds are common. Elongate nodules are 5–30 cm long, subvertical, and downward branching and tapering. Tabular nodules are 3–20 cm thick and up to 3 m long, bedding parallel, mainly in conglomerate, and commonly below equant and elongate nodules. Reddened sandstone plasma (soil matrix) is massive and cemented by calcite or iron oxide, with irregular or digitated base, suggesting downward illuviation (Fig. 3C). Muddy plasma has weekly to moderately calcareous peds that are platy, prismatic, or equant, angular to rounded, and ~2–30 mm in size. Slickensides are small and uncommon. Color mottles are rare to abundant, rounded, and have diffuse to sharp boundaries. Limestone alteration is indicated by autobrecciation, color mottling, patchy oxidation, and micritic crusts containing lithic grains. Downward tapering burrows filled with silt and sand are common but micro-karstic features are absent. Soil profiles are 10 cm to 2 m thick with common Bk, Bt, and BC horizons (Fig. 3G; Retallack, 1990) and are commonly stacked.

Histosols contain coal and interbedded carbonaceous shale and highly mottled mudstone. Coals are lignitic to sub-bituminous, 1–20 cm thick. Spodosols commonly cap fine-grained floodplain and deltaplain deposits and overlie Histosols if present. They are dark gray, brown, or variegated and contain no or minimal organic carbon. Common color mottles are rounded and mm in diameter; elongate, downward tapering mottles are cm long and locally concentrated. Some mottles have a dark-colored central spot, interpreted as stele. Horizons with iron-oxide pisoids are not uncommon (Figs. 3H, 4, 5). The pisoids are brown, rounded, 3–15 mm in diameter and non-calcareous. Cortices are discontinuous wavy laminae 1–10 microns thick, composed of hematite and goethite with scattered sand and silt grains; cores are dense ferruginous claystone. The pisoids-bearing horizon was interpreted as the Bs horizon (Retallack, 1990; Mack et al., 1993). It is 30–100 cm thick with pisoids concentrated in the middle, and commonly overlain by a 10 cm thick mudstone. Muddy plasma is non-calcareous. Peds are mostly rounded, equant to prismatic, 2–10 mm in size. Soil horizons are vague, except where Bs horizons are present. Soil profiles are 1–2 m thick and commonly stacked.

3. Depositional cycles and climate interpretation

372 primary depositional cycles were delineated and grouped into five types on the basis of facies association, depositional environments, and their systematic changes (Fig. 4). They are basic stratigraphic entities composed of both component lithofacies and bounding surfaces.

3.1. Braided stream cycles

These cycles contain crudely upward-fining conglomerate and sandstone of braided stream deposits commonly with erosional basal and top boundaries and are 1–11 m thick (Figs. 4, 5). The Kungurian cycles fill topographic lows on an unconformity (Figs. 3A, 5), forming an overall convex-upward geometry interpreted as an alluvial fan. The cycles in the basal Hongyanchi LC were deposited on an unconformity cutting into the Roadian lacustrine cycles (Figs. 3I, 5). The formation of the unconformities and ensuing deposition of braided stream systems suggest rejuvenated provenance uplift and/or spill point lowering (Figs. 4, 5). However, climate conditions during sedimentation can be speculated from climate-sensitive sedimentary features in the braided stream deposits.

Calcisols cap most cycles in the Upper Daheyan LC (Figs. 2, 3C, 5), suggesting a semi-arid climate (Retallack, 1990) where sedimentation was episodic and soil developed during prolonged hiatuses. Intra-cycle variation from a more humid condition during deposition to a more arid condition during soil formation may be present. It should be noted that in Figs. 4 and 5, the environmental curve correlates with

the lithologic column in the thickness domain, whereas the climate curve correlates with the entire cycle in the time domain, including the hiatus when deposition ceased and pedogenesis progressed. This dilemma of graphically presenting the two curves together exists in all cycle types for climate interpretation based on sedimentary features that were not formed syndepositionally. Absence of Calcisol cap in the braided stream cycles of the Lower and Middle Daheyan and basal Hongyanchi LCs (Figs. 2, 4, 5) indicates relatively continuous deposition by perennial streams and, thus, a high *P*/*E* ratio. Alternatively, it could have been caused by accelerated subsidence and, in the case of the basal Hongyanchi cycles, the lake termination could have been caused by tectonic uplift of the catchment basin or lowering of lake spill point. Rare Spodosol-capped braided stream cycles in the Wutonggou LC (Figs. 2, 4, 5) were interpreted as being deposited in a subhumid–humid climate.

3.2. Coarse-grained meandering stream cycles

These cycles contain thick channel-fill conglomerate and sandstone and thin overbank sandstone, mudrock, and paleosol of coarse-grained meandering stream deposits and erosional cycle boundaries (Fig. 4). They are 2–8 m thick (Fig. 5). The Calcisol-capped cycles in Lower–Middle Permian suggest a semi-arid–subhumid climate, whereas Histosol and Spodosol-capped cycles in Upper Permian suggest a subhumid–humid climate (Figs. 4, 5; Retallack, 1990). They generally overlie braided stream cycles and underlie classic meandering stream cycles (Miall, 1996) containing significant amount (>50%) of fine-grained overbank deposits. The stacking of the three types of fluvial cycles indicates stream evolution during expansion and peneplanation of catchment basin, provenance denudation, and increased stream discharge caused by an enlarged catchment and/or an increasingly humid climate.

3.3. Classic meandering stream cycles

These cycles consist of channel-lag conglomerate and sandstone and accretionary point bar sandstone in the lower part and thick overbank mudrock and paleosol in the upper part with erosional cycle boundaries (Figs. 3I, 4). They are 2–12 m thick, capped by Histosol and/or Spodosol, and alternate with deltaic cycles mainly in the Wuchiapingian Wutonggou LC (Fig. 5). This type of cycles, especially those thick (>10 m) "super" ones, suggests large perennial river flow in a large catchment basin, intense source denudation and weathering, and a humid–subhumid climate (Fig. 4; Miall, 1996). Common plant remains and petrified woods support this interpretation.

3.4. Lacustrine deltaic cycles

These cycles commonly contain a basal thin transgressive shoreline to littoral deposits of well-washed sandstone or conglomerate, a thick upward-coarsening and thickening prodeltaic-delta front succession of shale, sandstone, and/or conglomerate in the middle, and distributary channel and interdistributary deltaplain facies of sandstone, conglomerate, and mudrock in the upper part (Figs. 3D, 4). They are 1–13 m thick with sharp to erosional cycle boundaries (Fig. 5).

Initiation of a deltaic cycle containing a basal transgressive deposit overlying a fluvial cycle indicates lake deepening/expansion followed by contraction/shallowing. If the cycle overlies a lacustrine non-deltaic cycle, the deltaic cycle suggests increased influx of river water and sediments. The successively stacked deltaic cycles may be caused by fluctuation of river influx or delta lobe switching. In any case, delta progradation suggests large influx of river water and sediments and, thus, a high *P*/*E* ratio, although lake transgression may be of a tectonic, climatic, and/or autogenic origin. Common disseminated plants in prodeltaic and delta front facies and carbonaceous shale, Histosol, and Spodosol in deltaplain facies suggest continuing humid condition during deltaic deposition. The deltaplain Calcisols in the Roadian cycles, however, suggest intra-cycle climate changes from humid during lake expansion and delta progradation to subhumid/semi-arid at the end or after deltaic deposition (Figs. 4, 5).

3.5. Lacustrine mixed carbonate and siliciclastic cycles

These cycles have many facies varieties forming a basic trend of lake expansion-deepening and contraction-shallowing. These cycles are 0.2–3 m thick, abundant in the Roadian and Wordian intervals (Figs. 3E, 5). The basal coarse-grained deposits overlying fluvial or lakeplain facies are commonly well washed, suggesting a high-energy lake shore or littoral environment during lake expansion (Fig. 4). The middle sub-mm laminated organic-rich shale indicates a starved profundal environment during maximum expansion. The upper limestone and dolomitic shale/dolomite indicate a low-energy, increasingly saline and evaporative environment (see also Carroll, 1998). The capping Calcisol in parent mudrocks indicates lake withdrawal

and subaerial exposure. Absence of thick sandy deposits suggests under-filled to balance-filled lakes (Carroll and Bohacs, 1999) and an overall low *P*/*E* ratio. Intra-cycle variation of high-to-low *P*/*E* ratio correlates with lake expansion and contraction (Figs. 4, 5); interlaminations in shale and limestone suggest strong precipitation seasonality (Fig. 3F).

3.6. Multi-order cyclicity

Stratigraphic stacking of the five types of primary cycles shows three orders of cyclicity: primary high-order cycles, intermediate-order cycles (IC) composed of the same type of HCs or different types of HCs showing systematic thickness and/or facies changes, and low-order cycles composed of ICs formed in similar long-term tectonic and/or climatic conditions. The three orders of cycles reflect short, intermediate, and long-term environmental changes caused by interplay of autogenic and allogenic processes, and may not indicate solely cyclic climatic changes (Fig. 5). Examination of interpreted climate conditions of these cycles, however, suggests multi-order climatic variability.

4. Results and discussion

Climatic variability was identified at four levels: sub-cycle within HCs, and high, intermediate, and low-order cycle levels (Fig. 5), which constitute three orders of climate cycles. The climate cycles in many cases coincide with depositional cycles, but not in all cases for several reasons: (1) climate is not the sole control on cyclic sedimentation; (2) climate signals may be masked by other processes or not preserved; and (3) climate signals other than *P*/*E* ratio, such as temperature and wind, were not interpreted in this study. For example, changes in *P*/*E* ratio may not be present within a HC, such as a Histosol/Spodosol-capped deltaic cycle; the same depositional cycles may show different climatic variability, such as braided stream cycles with or without capping Calcisols (Fig. 4). Sub-cycle variability is generally small in magnitude and gradual in shift.

High-order climate variations across high-order depositional cycle boundaries overall have a small magnitude but abrupt shift (Fig. 5). The abrupt shift may be in part due to depositional hiatus at cycle boundaries (see also previous discussion on dilemma of graphic presentation). Intermediate-order variations commonly have a moderate to large magnitude across IC boundaries but small within (Fig. 5). ICs differ in thickness (3–189 m), overall *P*/*E* ratio, and its intra-cycle variations, suggesting highly variable cycle duration and climate conditions at the intermediate level.

Low-order climate cycles have abrupt climatic changes, which may be partially an artifact of unconformable cycle boundaries (Fig. 5). The thickness and climate variability vary greatly. The Kungurian Lower Daheyan LC contains six ICs composed of mainly coarse-grained meandering stream HCs, deposited in mainly subhumid climate with thin humid intervals (Figs. 2, 5). The Kungurian Middle and Upper Daheyan LCs contain at least two ICs (Fig. 2) composed of braided stream HCs. An abrupt shift from humid to subhumid-semi-arid conditions occurs at the base of the Middle Daheyan LC; and an abrupt shift to a semi-arid condition occurs across the top of the LC, as indicated by the first persistent occurrence of Calcisols (Fig. 5). An abrupt shift from semi-arid to subhumid conditions occurs at the top of the Upper Daheyan LC. An overall humid to semi-arid trend is present in the entire Kungurian interval (Fig. 5).

The Roadian Lucaogou LC contains 11 ICs and shows a highly variable climate. The lower five ICs show stepwise shift from semi-arid-subhumid to humid conditions with moderate variability, indicated by alternating thick deltaic HCs and thin mixed siliciclastic and carbonate HCs (Figs. 3D, 5). The upper six ICs show large shifts between semi-arid to humid conditions and strong precipitation seasonality at sub-cycle and HC scales (Fig. 3E). The Wordian Hongyanchi LC contains eight ICs. Large fluctuations at the IC scale are characterized by thick humid intervals and thin subhumid–semi-arid intervals, and by an overall shift to a semi-arid condition culminating at the end of Wordian (Figs. 3G, 5). The Capitanian Quanzijie LC is thin with two ICs (Figs. 2, 5). An abrupt semi-arid to humid–subhumid shift at the base is the beginning of a dominantly humid climate into the Late Permian (Fig. 5). The overall condition varies moderately between humid and subhumid, as indicated by thick highly oxidized lakeplain and overbank deposits (Fig. 5).

The Wuchiapingian Wutonggou LC is thick with nine ICs composed of alternating stacked classic meandering stream and deltaic HCs, deposited in humid–subhumid climate (Fig. 5). The lower five ICs are consistently humid. The upper four ICs show fluctuating humid–subhumid conditions. The great thickness of fluvial and deltaic deposits suggests intense provenance weathering and large sediment production and transport in the catchment basin, indicating persistent and constant provenance uplifting and basin subsidence and a strong wet–dry seasonality (Schumm, 1968; Miall, 1996). Preliminary field observations of

this and adjacent Taodonggou sections (Fig. 1B) indicate similar conditions in the rest of Upper Permian (e.g., Brand et al., 1993; Wartes et al., 2002; Yang et al., 2006).

The above continental climate record raises several questions. First is the origin(s) of climate variability. A detailed, reliable reconstruction should utilize multiple climate indicators, not sedimentary evidence alone. Thus, this reconstruction is only preliminary. Nevertheless, the presence of four-level climate variability is likely real and suggests hierarchical deterministic causes. Local and regional cycle correlation will likely identify local vs. regional climate variations and their controls (Yang et al., 2006). The intermontane setting of the studied strata suggests that orographic effect is a likely cause of some variations (Gibbs et al., 2002; see Hendrix et al., 1992 for Mesozoic examples in this region). Time series and spectral analyses of the cyclic record may test the link between depositional and climatic cyclicity and Milankovitch orbital forcing at the sub-cycle to IC scales (e.g., Olsen, 1986; Yang and Kominz, 1999).

Second, the late Kungurian–Wordian semi-arid conditions (Fig. 5) are in conflict with modern east-coast macrothermal humid climate at mid-latitudes (cf. Gibbs et al., 1993; Carroll, 1998; Zhu et al., 2005). Extreme continentality, orographic effect, and/or abnormal circulation of Panthalassa (e.g., Gibbs et al., 2002) may be possible causes. Our work serves as a rare data point at mid-latitudes for future climate modeling to seek explanations.

Finally, the Roadian–Wordian highly variable climate contrasts sharply with the Capitanian–Wuchiapingian stable humid climate. The contrast was also suggested by organic carbon isotope data in the region (Foster and Metcalfe, 2002). It, combined with abundant fish fossils in the Roadian–Wordian deposits (e.g., Liao et al., 1987) that indicate mass mortality, suggests that terrestrial mass extinction may have started in the Roadian, strengthened in Late Permian, and climaxed at the end-Permian (cf. Ward et al., 2005).

5. Conclusions

Four levels of mid-latitude climate variability in *P*/*E* ratio were interpreted preliminarily from climate-sensitive sedimentary indicators and the type and stacking pattern of depositional cycles of Lower–Upper Permian fluvial–lacustrine strata in NW China. Early Kungurian climate fluctuated between subhumid to humid at the IC scale, and shifted gradually to semi-arid in late Kungurian. Roadian climate fluctuated widely from humid to semi-arid with strong precipitation seasonality at sub-cycle and HC scales. Wordian climate changed to dominantly humid with thin subhumid intervals and ended with a peak semi-arid condition. Capitanian climate was mainly subhumid-humid, starting a thick interval of stable, dominantly humid and highly seasonal climate through the Wuchiapingian time. The late Kungurian–Wordian semi-arid climate is incompatible with modern mid-latitude east-coast humid climate, suggesting that different mechanisms, such as orography, extreme continentality, and abnormal oceanic circulation, may have been active in Pangea and Panthalassa. Finally, the highly variable Roadian–Wordian climate may have started terrestrial mass extinction that climaxed at the end of Permian.

Acknowledgements

We thank Z.J. Ouyang, W.H. Ma, H.Y. Wu, M. Runnion, H.Y. Wang, and X.J. Xin for field assistance. Reviews by Dr. N. Tabor and, especially, Dr. M. Hendrix greatly improved the science of the paper. We thank Dr. D. Lehrmann for editorial support. The project was partially supported by three grants from Wichita State University and two grants from the Key Laboratory of Continental Dynamics, Northwestern University, China, all to WY. WY also gratefully acknowledges the support of K. C. Wong Education Foundation, Hong Kong, obtained through the collaboration with Dr. X.R. Luo of Institute of Geology and Geophysics, Chinese Academy of Sciences, and support from the Knowledge Innovation Project of Chinese Academy of Sciences (key project No. 80567300).

References

Allen, M.B., Sengor, A.M.C., Natal'in, B.A., 1995. Junggar, Turfan and Alakol basins as Late Permian to ?Early Triassic extensional structures in a sinistral shear zone in the Altaid orogenic collage, Central Asia. J. Geol. Soc. (Lond.) 152, 327–338.

Brand, U., Yochelson, E.L., Eagar, R.M., 1993. Geochemistry of Late Permian non-marine bivalves: implications for the continental paleohydrology and paleoclimatology of northwestern China. Carbonates Evaporites 8, 199–212.

Carroll, A.R., 1998. Upper Permian lacustrine organic facies evolution, southern Junggar Basin, NW China. Org. Geochem. 28, 649–667.

Carroll, A.R., Bohacs, K.M., 1999. Stratigraphic classification of ancient lakes: balancing tectonic and climatic controls. Geology 27, 99–102.

Carroll, A.R., Graham, S.A., Hendrix, M.S., Ying, D., Zhou, D., 1995. Late Paleozoic tectonic amalgamation of northwestern China: sedimentary record of the northern Tarim, northwestern Turpan, and southern Junggar Basins. Geol. Soc. Amer. Bull. 107, 571–594.

Erwin, D.H., 1993. The great Paleozoic crisis: life and death in the Permian. In: Bottjer, D.J., Bambach, R.K. (Eds.), Critical Moments in Paleobiology and Earth History Series. Columbia Univ. Press, New York, pp. 23–44.

Erwin, D.H., 2002. Testing alternative scenarios for the end-Permian extinction. Geol. Soc. of Australia, Abstracts Number 68, First Inter. Palaeontological Congress (IPC2002), p. 50.

Foster, C., Metcalfe, I., 2002. Carbon isotopic composition of organic matter from non-marine Permian–Triassic boundary sections at Dalongkou and Lucaogou, Xinjiang, NW China. Geol. Soc. of Australia, Abstracts Number 68, First Inter. Palaeontological Congress (IPC2002), pp. 56–57.

Gibbs, M.T., Rees, P.Mc., Kutzbach, J.E., Ziegler, A.M., Behling, P.J., Rowley, D.B., 2002. Simulations of Permian climate and comparison with climate-sensitive sediments. J. Geol. 110, 33–55.

Greene, T.J., Carroll, A.R., Wartes, M., Graham, S.A., Wooden, J.L., 2005. Integrated provenance analysis of a complex orogenic terrane: mesozoic uplift of the Bogda Shan and inception of the Turpan-Hami Basin, NW China. J. Sediment. Res. 75, 251–267.

Hendrix, M.S., Graham, S.A., Carroll, A.R., Sobel, E.R., McKnight, C.L., Schulein, B.J., Wang, Z., 1992. Sedimentary record and climatic implications of recurrent deformation in the Tian Shan: evidence from Mesozoic strata of the north Tarim, south Junggar, and Turpan basins, northwest China. Geol. Soc. Amer. Bull. 104, 53–79.

Isozaki, Y., 1997. Permo–Triassic boundary superanoxia and stratified superocean: records from the lost deep sea. Science 276, 235–238.

Knoll, A.H., Bambach, R.K., Canfield, D.E., Grotzinger, J.P., 1996. Comparative Earth history and the Late Permian mass extinction. Science 273, 452–457.

Liao, Z., Lu, L., Jiang, N., Xia, F., Song, F., Zhou, Y., Li, S., Zhang, Z., 1987. Carboniferous and Permian in the western part of the east Tianshan Mountains. Eleventh Congress of Carboniferous Stratigraphy and Geology, Guidebook Excursion 4, Beijing, China. 50 pp.

Mack, G.H., James, W.C., Monger, H.C., 1993. Classification of paleosols. Geol. Soc. Amer. Bull. 105, 129–136.

Miall, A.D, 1996. The Geology of Fluvial Deposits: Sedimentary Facies, Basin Analysis, and Petroleum Geology. Springer, New York. 582 pp.

Olsen, P.E., 1986. A 40-million-year lake record of Early Mesozoic orbital climatic forcing. Science 234, 842–848.

Retallack, G.J., 1990. Soils of the Past—An Introduction to Paleopedology. Unwin Hyman, Boston. 520 pp.

Schumm, S.A., 1968. Speculations concerning paleohydrologic controls of terrestrial sedimentation. Geol. Soc. Amer. Bull. 79, 1573–1588.

Scotese, C.R., McKerrow, W.S., 1990. Revised world maps and introduction. In: McKerrow, W.S., Scotese, C.R. (Eds.), Palaeozoic Palaeogeography and Biogeography. Geological Society Memoir, vol. 12, pp. 1–21.

Shao, L., Stattegger, K., Li, W., Haupt, B.J., 1999. Depositional style and subsidence history of the Turpan Basin (NW China). Sediment. Geol. 128, 155–169.

Shao, L., Stattegger, Garbe-Schoenberg, C.-D., 2001. Sandstone petrology and geochemistry of the Turpan Basin (NW China): implications for the Tectonic evolution of a continental basin. J. Sediment. Res. 71, 37–49.

Ward, P.D., Botha, J., Buick, R., De Kock, M.O., Erwin, D.H., Garrison, G.G., Kirschvink, J.L., Smith, R., 2005. Abrupt and gradual extinction among Late Permian land vertebrates in the Karoo Basin, South Africa. Science 307, 709–714.

Wartes, M.A., Carroll, A.R., Greene, T.J., 2002. Permian sedimentary record of the Turpan-Hami Basin and adjacent regions, Northwest China; constraints on postamalgamation tectonic evolution. Geol. Soc. Amer. Bull. 114, 131–152.

Yang, W., Kominz, M., 1999. Testing periodicity of depositional cyclicity, Cisco Group (Virgilian and Wolfcampian), Texas. J. Sediment. Res. 69B, 1209–1231.

Yang, W., Liu, Y.Q., Qiao, F., Zhou, D.W., Wang, D., Runnion, M., 2006. Middle Permian to Lower Triassic fluvial–lacustrine depositional systems and sequence stratigraphy, Bogda Mountains, Turpan Intermontane Basin, NW China. 2006 American Association of Petroleum Geologists Annual Meeting, Abstract Volume, p. 117.

Zhu, H.-C., Ouyang, S., Zhan, J.-Z., Wang, Z., 2005. Comparison of Permian palynological assemblages from the Junggar and Tarim basins and their phytoprovincial significance. Rev. Palaeobot. Palynol. 1363, 181–207.

Ziegler, A.M., Hulver, M.L., Rowley, D.B., 1997. Permian world topography and climate. In: Martini, I.P. (Ed.), Late Glacial and Postglacial Environmental Changes: Pleistocene, Carboniferous–Permian, and Proterozoic. Oxford Univ., Oxford, pp. 111–146.

Zhang, X., 1981. Regional Stratigraphic Chart of Northwestern China, Branch of Xinjiang Uygur Autonomous Region. Geological Publishing House, Beijing. 496 pp. (in Chinese).